

Beacon-enabled TDMA Ultraviolet Communication Network System Design and Realization

Yuchen Pan¹, Fei Long¹, Ping Li², Haotian Shi², Jiazhao Shi², Hanlin Xiao², Chen Gong^{1,*}, and Zhengyuan Xu¹

¹key Laboratory of Wireless-Optical Communications, Chinese Academy of Sciences, School of Information Science and Technology, University of Science and Technology of China, Hefei, Anhui 230026, China

²Xi'an Modern Control Technology Research Institute, Xi'an 710065

*Corresponding author: cgong821@ustc.edu.cn

Abstract—Nonline of sight (NLOS) ultraviolet (UV) scattering communication can serve as a good candidate for outdoor optical wireless communication (OWC) in the cases of non-perfect transmitter-receiver alignment and radio silence. We design and demonstrate a NLOS UV scattering communication network system in this paper, where a beacon-enabled time division multiple access (TDMA) scheme is adopted. In our system, LED and PMT are employed for transmitter and receiver devices, respectively. Furthermore, we design algorithms for beacon transmission, beacon reception, time compensation, and time slot transition for hardware realization in field-programmable gate array (FPGA) board based on master-slave structure, where master node periodically transmits beacon signals to slave nodes. Experimental results are provided to evaluate the time synchronization error and specify the system key parameters for real-time implementation. We perform field tests for real-time communication network with the transmission range over $110 \times 90\text{m}^2$, where the system throughput reaches 800kbps.

Index Terms—wireless communication network, UV scattering communication system, beacon, time synchronization, master-slave structure

I. INTRODUCTION

Non-line of sight (NLOS) scattering communication can offer optical wireless communication link for radio-silence scenarios while not requiring perfect alignment of the transmitter and receiver [1]–[4]. Existing works based on NLOS visible light communication (VLC) have been reported in [5]–[7]. However, NLOS VLC suffers from strong solar interference especially during daytime. Compared with VLC, NLOS ultraviolet (UV) communication is adopted in outdoor environments during daytime since the background radiation of UV spectrum within spectrum between 200nm and 280nm is absorbed by the atmosphere [2]. Hence, the characteristics of UV [8] leads to prospective application of UV communication in the case of non-perfect transmitter-receiver alignment and strong background radiation.

NLOS UV scattering communication has been extensively investigated from theoretic and experimental perspectives. Different from RF-based communication, the received signal of UV communication exhibits the characteristics of discrete photoelectrons due to the extreme path loss. Hence, the Poisson-type channel has been adopted for investigating UV channel capacity and achievable rate. The capacities of Poisson channel have been studied in [9]–[15]. The capacities of continuous-

time and discrete-time Poisson channel have been investigated in [9], [10] and [11], [12], respectively. The capacity of MISO has been reported in [13]. Moreover, the capacities of Poisson fading channel and MIMO Poisson fading channel have been studied in [15] and [14], respectively. Regarding UV channel link gain, existing works based on the UV channel model have been reported in [16]–[19], which have investigated the channel link gain from Monte Carlo, theoretic and experimental perspective. Furthermore, the characterization and detection of the UV receiver-side signal have been studied in [20]–[23]. Channel estimation of UV channel parameters have been investigated in [21], [23], while the characterization on practical photon counting receiver has been discussed in [20] and the signal detection for optical scattering communication in different scenarios have been studied in [21], [22]. Other physical layer techniques have been reported in [24], [25], including polar codes in wireless communications [24] and spectrum sensing for optical wireless scattering communications [25]. Besides the theoretical investigation, experimental works on UV scattering communications have been discussed in [26]–[29].

UV communication networks are widely investigated for a network scenario to enhance system performance. The Poisson multiple access channel has been investigated in [30]. The connectivity performance for UV networks has been studied in [31]. Existing works based on the medium-access control (MAC) techniques for UV communication networks have been reported in [32], [33], while signal characterization and detection for multiple access NLOS communication have been investigated in [34], [35].

In this paper, we realize the real-time UV time division multiple access (TDMA) communication network, consisting one master node and multiple slave nodes, over $90 \times 100\text{m}^2$ with over 800 kbps throughput via applying beacon-based time synchronization. We employ a UV LED as the transmitter and photomultiplier tubes (PMTs) as the receiver. We design and realize signal processing algorithms based on the discrete-time Poisson channel model, consisting of beacon transmission, beacon reception, time compensation and time slot transition. Experiments are conducted to measure the time synchronization error between nodes such that the guard intervals can be designed to avoid collision. Furthermore, we realize a real-time 4-node UV communication network system consisting

of multiple PMTs, field-programmable gate array (FPGA) boards for implementation of digital signal processing. We complete a real-time UV network communication experiment with the transmission range over $90 \times 100m^2$ and the resulting throughput can reach 800 kbps.

This remainder is organized as follows. In Section II, we provide the block diagrams of the proposed communication network system. In Section III, we address the signal processing of beacon-based time synchronization and time slot transition. Experimental results are shown in Section IV. Finally, we conclude this paper in Section V.

II. SIGNAL CHARACTERIZATION AND SYSTEM BLOCK DIAGRAM

A. Signal Characterization of UV Communication

We adopt UV spectrum for communication due to its scattering property to enhance system reception range and limited transmission distance to enhance security. The received signals at the receiver side are in the discrete-photon level in the form of photoelectrons, whose number satisfies Poisson distribution. Let N_i denote the number of received photoelectrons from node i within symbol duration and S denote the transmitted symbol. N_i satisfies the following Poisson distribution:

$$P(N_i = n | S = 1) = \frac{\lambda_{s,i} + \lambda_{b,i}^n}{n!} e^{-\lambda_{s,i} - \lambda_{b,i}}, \quad (1)$$

$$P(N_i = n | S = 0) = \frac{\lambda_{b,i}^n}{n!} e^{-\lambda_{b,i}}, \quad (2)$$

where $\lambda_{s,i}$, $\lambda_{b,i}$ denote the mean number of received photoelectrons at node i for the signal and background components.

B. Wireless Communication Network System Block Diagram

We consider a N -node network, consisting of one master node (denoted as node 1) and $(N - 1)$ slave nodes (denoted as node 2, 3, \dots , N , respectively). Each node works as a transceiver. Any two nodes can communicate with each other through one hop. TDMA MAC scheme is adopted. The master node broadcasts beacon signal to the slave nodes. Each node accesses the channel according to the allocated slot after time synchronization is performed by the slave nodes based on the beacon signal reception. An example of 4-node network is shown in Fig. 1 to show the topology and the data flow of the network system.

The FPGAs are adopted as the data processing unit of each node. The information bits are randomly generated in the personal computer(PC). The information bits are divided into groups of 8 bits and sent from the PC to the FPGA board via UART interface. In addition, the beacon signals are generated in the FPGA board of the master node. LEDs are employed as the UV transmitter and we adopt OOK modulation. The information bits and beacon signals are exported to modulate the UV LED via the pin of the FPGA board.

PMTs are employed as the photon-detector, which can convert the received photoelectrons to analog pulses such that photon counting can be realized via pulse counting. A PMT(CR340) detector is sealed into a shielding box, which is integrated with a UV optical filter that passes the light

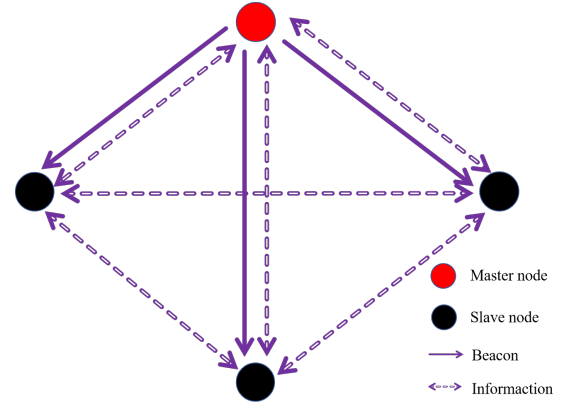


Fig. 1. Example of a network topology.

signal of wavelength around 266 nm and blocks signals on other wavelengths. The digital voltage values are achieved via analog-to-digital converters(ADCs). The digital processing of beacon reception, time compensation, time slot transition is performed in the FPGA boards of the slave nodes and the digital processing of frame synchronization, channel estimation and symbol detection are performed in the FPGA boards of all nodes. The block diagram and experimental system of the NLOS UV scattering communication network are shown in Figs. 2 and 3, respectively.

III. DIGITAL PROCESSING IN HARDWARE REALIZATION

A. Beacon Transmission

The master node automatically transmits periodic beacon signal with period T to the slave nodes after FPGA board of the master node working. We adopt L -bit binary m sequence as the beacon signal due to its excellent autocorrelation.

The time counter of the master node will start working as it starts transmitting beacon signal. Let C_i denote the time counter of node i . C_1 counts from 0 to $(C_{max} - 1)$ periodically, where $C_{max} \times t_{clock} = T$ and t_{clock} denotes the interval of two consecutive clock rising edge.

The time synchronization pulses are generated by the slave nodes via finding the start of beacon signal such that the slave nodes can achieve time synchronization as the master node. We divide the received signals into chips with the duration $T_c = \frac{T_s}{M}$, where T_s denotes the symbol duration and M denotes the number of chips in one symbol. The counting-based synchronization in [36] is adopted for beacon reception. The position with the maximum correlation peak corresponds to the start of beacon signal.

B. Time Compensation and Time Slot Transition

1) *Time Delay Analysis*: Based on the details in III-A, the time delay between beacon transmission and time synchronization pulse generation consists of transmission delay t_{trans} , propagation delay t_{pro} and processing delay t_{ps} , as shown in Fig. 4. t_{trans} and t_{pro} are defined as in:

$$t_{trans} = L \times T_s, \quad (3)$$

$$t_{pro}^{ij} = \frac{r_{ij}}{C}, \quad 1 \leq i, j \leq N, i \neq j, \quad (4)$$

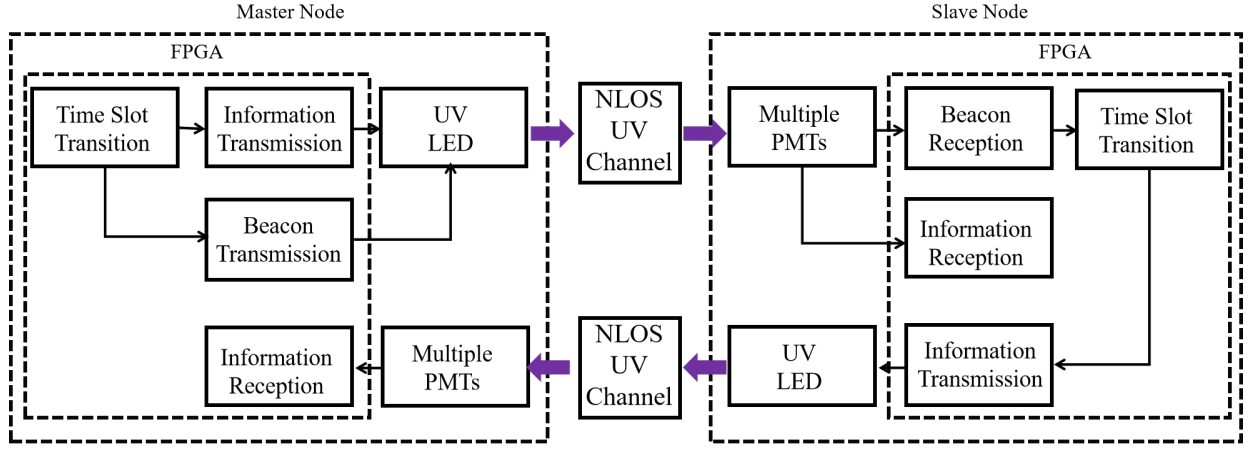


Fig. 2. The block diagram of NLOS UV Network System.

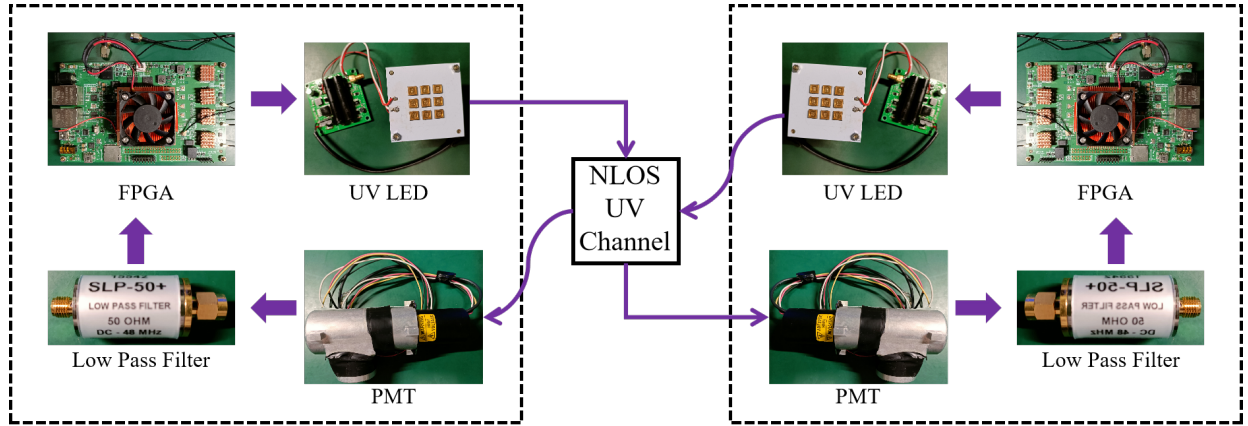


Fig. 3. The hardware realization blocks of the NLOS scattering communication network system.

where t_{pro}^{ij} denotes propagation between node i and j , C denotes the speed of light, and r_{ij} denotes the distance between node i and j , respectively. The processing delay should be experimentally measured since it is a random variable and is difficult to analyze via mathematical model. Let t_{ps}^i denote the processing delay of node i . Without loss of generality, assume that $t_{ps}^i, 1 \leq i \leq N$ are independent and identically distributed.

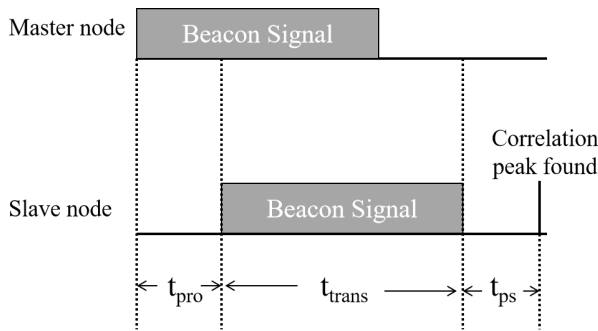


Fig. 4. Demonstration of three time delays.

2) *Time Compensation*: The time counters of the slave nodes start to count as the time synchronization pulses are achieved by the slave nodes. If the time counters of the slave nodes count from 0, the time delay shown in III-B1 will still

exist. The time compensation should be performed at the slave nodes due to the time delay. Instead of 0, $C_i, i = 2, 3, \dots, N$ will be set to the initial value $c_{initial}$ as the time synchronization pulse is generated by node i . $c_{initial}$ is defined as:

$$c_{initial} = \frac{t_{trans} + \max_j t_{pro}^{1j} + t_{ps}^{\sim}}{t_{clock}} \quad (5)$$

where t_{ps}^{\sim} denotes the experimentally measured processing delay. Let t_d^i denote the time synchronization error between node i and the master node, t_d^i is defined as :

$$t_d^i = \begin{cases} (t_{ps}^{\sim} - t_{ps}) + (\max_j t_{pro}^{1j} - t_{pro}^{1i}) & , 2 \leq i \leq N, \\ 0 & , i = 1. \end{cases} \quad (6)$$

3) *Time Slot Transition*: Each time period is divided into multiple slots based on TDMA MAC scheme. The time period of the master node consists of 1 beacon transmission slot, 1 beacon interval slot, $N \times (N - 1)$ information transmission slots and $N \times (N - 1)$ guard interval slots. Compared with the master node, the slave nodes don't have the beacon transmission slot. The slot transition depends on the time counter of each node. The time slot transition of the master node and the slave nodes is shown in Fig. 5. Let BT , BI denote beacon transmission slot, beacon interval slot, respectively.

The beacon transmission slot is for the master node to transmit beacon signal to the slave nodes, and the beacon interval slot is for the slave nodes to decode the beacon signal. Let t_{bt} and t_{bi} denote the duration of the beacon transmission slot and the duration of the beacon interval slot, respectively. t_{bt} and t_{bi} are subject to :

$$t_{bt} = L \times T_s, \quad (7)$$

$$t_{bi} \geq (\max_j t_{pro}^{1j} + t_{ps}^{\sim}), \quad (8)$$

$$t_d^i \leq |t_{bi} - (\max_j t_{pro}^{1j} + t_{ps}^{\sim})|. \quad (9)$$

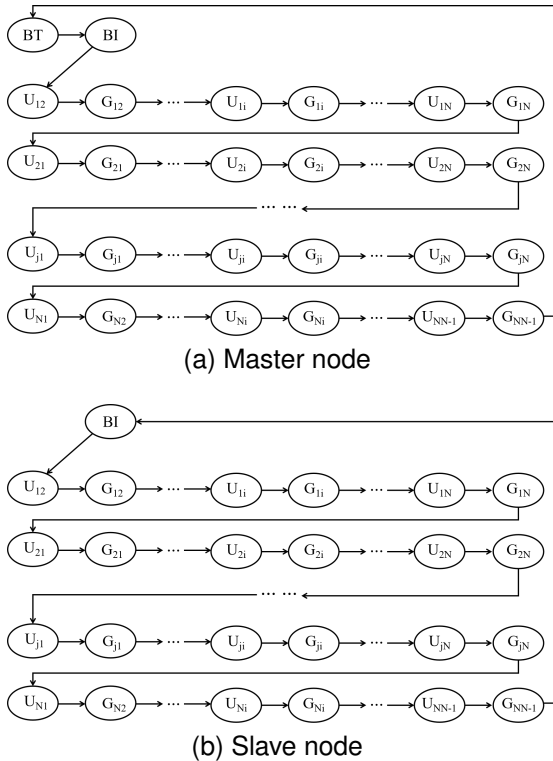


Fig. 5. State transition of the master node and the slave nodes.

The information slots are designed for nodes in the network to transmit information frames. U_{ij} in Fig. 5 denotes the time slot for node i transmitting frames to node j . The guard intervals are designed to avoid the collision caused by time synchronization error of different nodes. G_{ij} in Fig. 5 denotes the guard interval after time slot U_{ij} . Without generality, all guard intervals and information slots are set as the same length. Let t_g denote the duration of the guard interval and t_g is subject to :

$$t_g \geq |t_d^i - t_d^j|, \forall 1 \leq i, j \leq N. \quad (10)$$

Fig. 6 demonstrates the necessity of the guard interval. Based on the above demonstration, the time slot transition conditions of master node and slave node k are given in Equation. (11)-(19) and Equation. (20)-(27), respectively, where t_u denotes the length of one information slot.

IV. SYSTEM DESIGN WITH EXPERIMENTAL RESULTS

A. System Specification with Experimental Results

We specify the NLOS UV communication system under consideration. Let the number of beacon signal bits $L = 256$, the transmission symbol rate of OOK modulation $R_s = \frac{1}{T_s} = 2\text{Mbps}$, the number of chips within a symbol duration $M = 10$, and the time synchronization period $T=1\text{s}$. According to 8 and 10, the beacon interval and guard intervals are set to avoid the time slot overlap between different nodes. Hence, the time synchronization error test is conducted to specify the length of the beacon interval and guard intervals.

We conduct real-time lab test on the time synchronization error according to the scenario shown in Fig. 7. A start pulse P_m is generated by the FPGA board of the master node as it transmits the beacon signals. Synchronization pulses P_s are generated by the FPGA boards of the slave nodes as the slave nodes receive the beacon signals successfully. We can observe the time difference of the nodes via observing the distance of the pulses on the oscilloscope.

We show the time synchronization error in Fig. 8. The time pulses of two slave nodes overlaps due to the display scale of the oscilloscope. We adopt the independent repeated trials to achieve the distribution of the time synchronization error. We measure the time synchronization error 100 times and the distribution of the time synchronization error is shown in Fig. 10. The statistical variance and expectation of the time synchronization error are 0.015 and 132.941us, respectively. Moreover, it can be observed from the measured data that the maximum value of the data is less than 133us. Hence, $c_{initial}$ is set as $1.33e-4\text{s}$ to avoid the time collision between the master node and the slave nodes. The results after time compensation are shown in Fig. 9. The green pulse, blue pulse and red pulse denote the time of the master node, slave node 1 and slave node 2, respectively. It can be observed that the time synchronization errors between master node and slave nodes drops from 100-microsecond order to 50-nanosecond order. We consider t_{bi} to be set to 128us for processing, which is subject to Eq. (8). The length of all types of time slots is shown in Table I.

TABLE I
THE LENGTH OF ALL TYPES OF TIME SLOTS

Type of time slot	Length/symbol
Beacon transmission	256
Beacon interval	256
Information transmission	137500
Guard interval	29124

B. Lab Test on the Communication Network Performance

We conduct real-time lab test on the system performance with the designed system parameters from the experimental results in Table I and the devices specified in Table II. The experiment scenario is shown in Fig. 11. We consider four communication nodes, consisting of one master node and three slave nodes. All nodes are put towards the white wall of lab. UV light from the LEDs is reflected off the white wall to

$$BT \rightarrow BI : C_1 = \frac{t_{bt}}{t_{clock}}, \quad (11)$$

$$BI \rightarrow U_{12} : C_1 = \frac{t_{bt} + t_{bi}}{t_{clock}}, \quad (12)$$

$$U_{ij} \rightarrow G_{ij} : C_1 = \frac{t_{bt} + t_{bi} + ((i-1)(N-1) + (j-1))(t_u + t_g) + t_u}{t_{clock}}, 1 \leq j \leq i-1, 2 \leq i \leq N, \quad (13)$$

$$C_1 = \frac{t_{bt} + t_{bi} + ((i-1)(N-1) + (j-2))(t_u + t_g) + t_u}{t_{clock}}, i+1 \leq j \leq N, 1 \leq i \leq N-1, \quad (14)$$

$$G_{ij} \rightarrow U_{i(j+1)} : C_1 = \frac{t_{bt} + t_{bi} + ((i-1)(N-1) + j)(t_u + t_g)}{t_{clock}}, 1 \leq j \leq i-1, 2 \leq i \leq N, \quad (15)$$

$$C_1 = \frac{t_{bt} + t_{bi} + ((i-1)(N-1) + (j-1))(t_u + t_g)}{t_{clock}}, i+1 \leq j \leq N, 1 \leq i \leq N-1, \quad (16)$$

$$G_{i(i-1)} \rightarrow U_{i(i+1)} : C_1 = \frac{t_{bt} + t_{bi} + N(i-1)(t_u + t_g)}{t_{clock}}, 2 \leq i \leq N-1, \quad (17)$$

$$G_{iN} \rightarrow U_{(i+1)1} : C_1 = \frac{t_{bt} + t_{bi} + i(N-1)(t_u + t_g)}{t_{clock}}, 1 \leq i \leq N-1, \quad (18)$$

$$G_{N(N-1)} \rightarrow BT : C_1 = \frac{t_{bt} + t_{bi} + N(N-1)(t_u + t_g)}{t_{clock}}. \quad (19)$$

$$BI \rightarrow U_{12} : C_k = \frac{t_{bt} + t_{bi}}{t_{clock}}, \quad (20)$$

$$U_{ij} \rightarrow G_{ij} : C_k = \frac{t_{bt} + t_{bi} + ((i-1)(N-1) + (j-1))(t_u + t_g) + t_u}{t_{clock}}, 1 \leq j \leq i-1, 2 \leq i \leq N, \quad (21)$$

$$C_k = \frac{t_{bt} + t_{bi} + ((i-1)(N-1) + (j-2))(t_u + t_g) + t_u}{t_{clock}}, i+1 \leq j \leq N, 1 \leq i \leq N-1, \quad (22)$$

$$G_{ij} \rightarrow U_{i(j+1)} : C_k = \frac{t_{bt} + t_{bi} + ((i-1)(N-1) + j)(t_u + t_g)}{t_{clock}}, 1 \leq j \leq i-1, 2 \leq i \leq N, \quad (23)$$

$$C_k = \frac{t_{bt} + t_{bi} + ((i-1)(N-1) + (j-1))(t_u + t_g)}{t_{clock}}, i+1 \leq j \leq N, 1 \leq i \leq N-1, \quad (24)$$

$$G_{i(i-1)} \rightarrow U_{i(i+1)} : C_k = \frac{t_{bt} + t_{bi} + N(i-1)(t_u + t_g)}{t_{clock}}, 2 \leq i \leq N-1, \quad (25)$$

$$G_{iN} \rightarrow U_{(i+1)1} : C_k = \frac{t_{bt} + t_{bi} + i(N-1)(t_u + t_g)}{t_{clock}}, 1 \leq i \leq N-1, \quad (26)$$

$$G_{N(N-1)} \rightarrow BI : \text{The beacon signal of new period is decoded.} \quad (27)$$

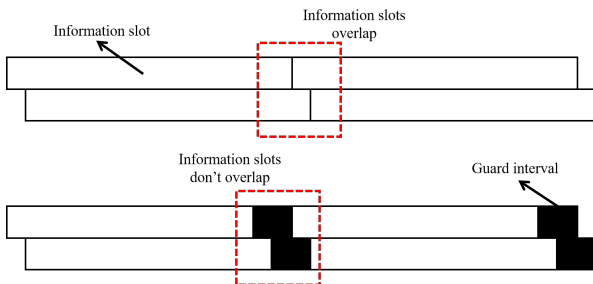


Fig. 6. Comparison between "with guard interval" and "without interval".

the received area of the PMTs. Each node transmits 10000 frames to the other nodes. The experimental results are shown in Fig. 12. "Frame_corret_num" and "Frame_receive_num" denote the number of successfully decoded frames and the

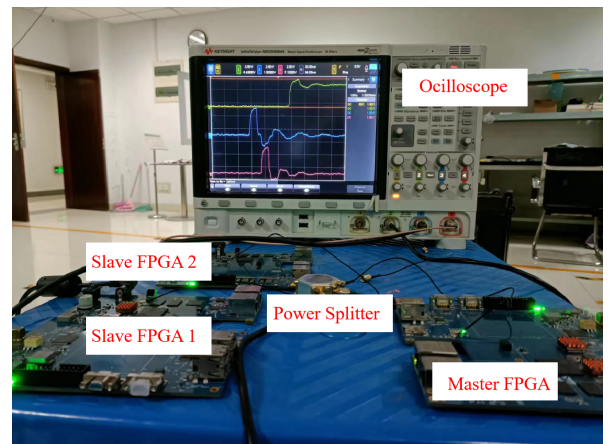


Fig. 7. The experimental scenario of time synchronization error test.



Fig. 8. Time synchronization error between nodes.

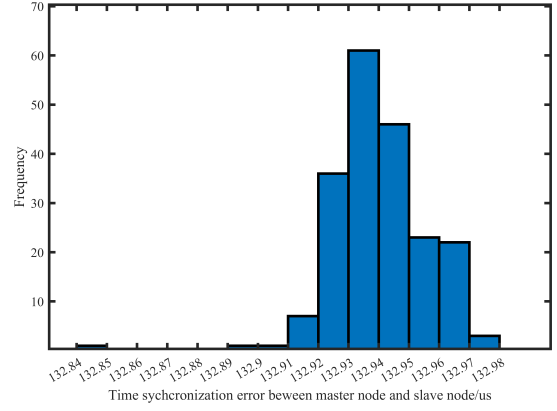


Fig. 9. Time synchronization error between nodes after time compensation.

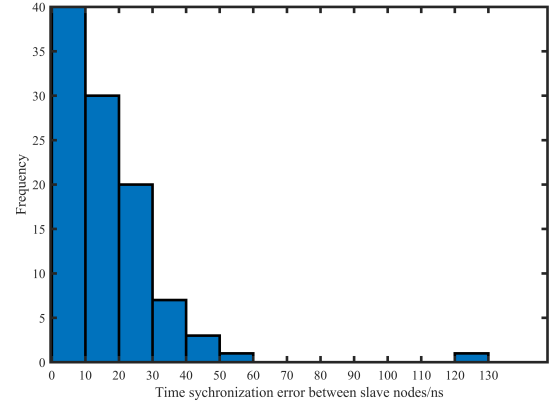
number of received frames, respectively. It can be observed that 40000 frames are received and decoded successfully by one node, which demonstrates that the UV network system can work under lab scenario.

TABLE II
SPECIFICATION OF EXPERIMENTAL EQUIPMENTS AND DEVICES

UV LED	Wavelength	266nm
	Electric power	58W
	Beam divergence	120°
UV optical filter	Peak wavelength	264nm
	Peak transmission	28.2%
	Full width at half maximum	20nm
	Aperture size	Φ31.5mm × 28.3mm
PMT	Spectral response	From 160nm to 320nm
	Quantum efficiency	Around 30% at 264nm
	Dark counts	≤ 10 per second
	Anode pulse rise time	2.2ns
	Detection bandwidth	≥ 200MHz
	Aperture size	Φ32.2mm × 94mm



(a) Error between master node and slave node



(b) Error between slave nodes

Fig. 10. Empirical probability distribution of time synchronization.

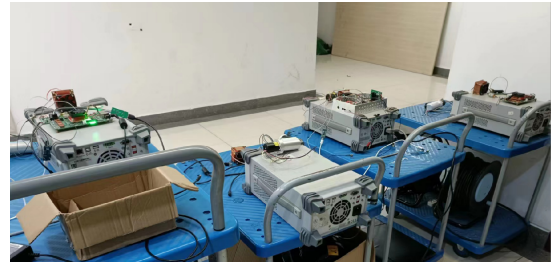


Fig. 11. Lab test scenario.

C. Transmitter-receiver Field of View (FOV) Test with Experimental Results

We conduct transmitter-receiver field of view test on the NLOS channel link gain with the specified parameters in Table I and devices in Table II before outdoor real-time field test to determine the quantity of PMTs for one node K . The geometric configuration of the transmitter and receiver is shown in Fig. 13. The transmitter position is set to be $(0, 0)$ and the receiver position is set to be $(0, 100)$. l and l' denote the orientation of the LED and PMT, respectively. Moreover, θ and θ' denote the rotation angle of the LED and PMT. We achieve the NLOS channel link gain with θ from 0° to 75° and θ' from 0° to 40° . The results are shown in Fig. 14. It is observed that Nlos channel link gain is significantly sensitive

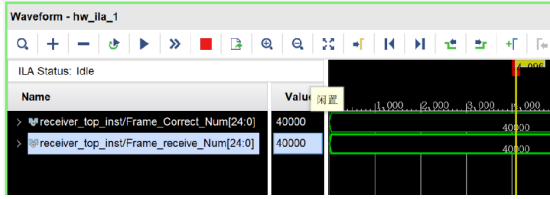


Fig. 12. The experimental results of lab test.

to the rotation of PMT due to the narrow FOV of PMT. The NLOS channel link gain dramatically drops below 4 while $\theta' = 30^\circ$, where the bit error rate (BER) of the communication link can not meet communication requirements.

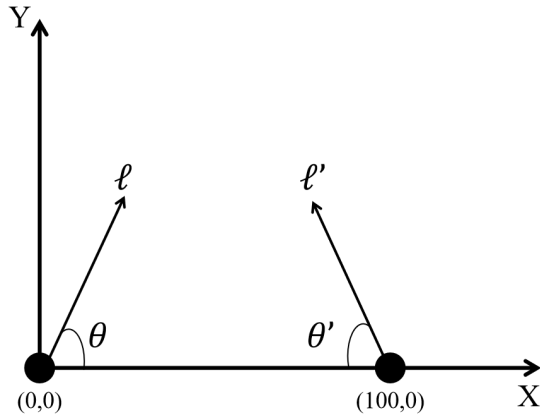


Fig. 13. FOV test scenario.

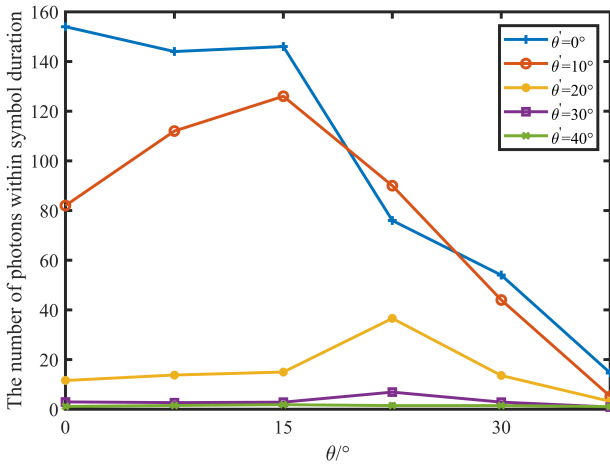


Fig. 14. NLOS channel link gain with different rotations of LED and PMT.

D. Field Test over $110 \times 90m^2$

Based on above experimental results in IV-C, we adopt the number of PMTs $K = 3$ while the number of nodes in the network $N = 4$. We carried out the outdoor field test on the real-time communication network consisting of one master node and three slave nodes. The network system layout is shown in Fig. 15. The location of the system was placed in school playground. The date of outdoor field test was

Oct.12th in 2023, where the weather conditions were 14°C - 23°C , cloudy, and eastern wind of 2 m/s. The four nodes are located at the four vertices of the rectangle. The width of school playground is about 90 meters while the length of the rectangle is about 110 meters. We show the hardware test bed of each node in Fig. 16. The three PMTs of each node were placed towards two right-angle sides and diagonal line as in Fig. 15, respectively. Each node transmits 10000 frames. We adopt the ila core in the Vivado to obtain the results. The experimental results are shown in Fig. 17, where "Frame_correct_num" and "Frame_receive_num" denote the number of successfully decoded frames and the number of received frames, respectively. It can be observed that each node can successfully decode all the transmitted frames from the other nodes.

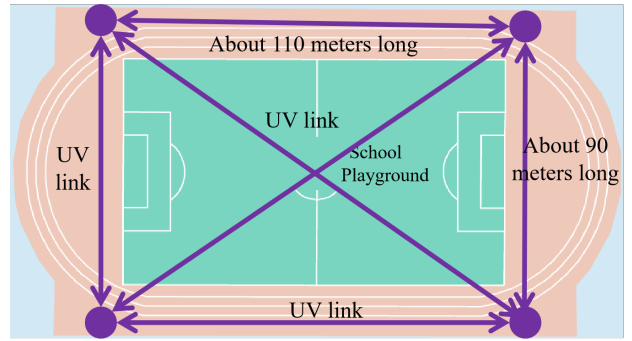


Fig. 15. The network system layout.

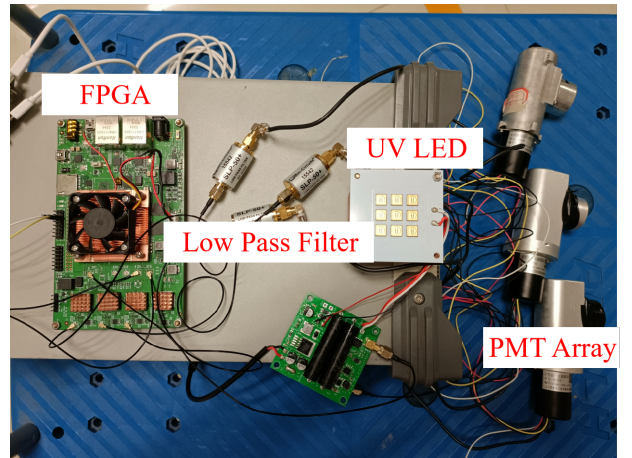


Fig. 16. The test bed of each node.

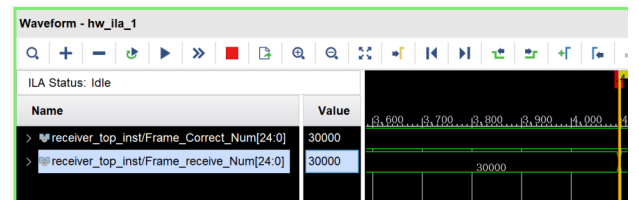


Fig. 17. The experimental results of field test.

V. CONCLUSION

We have designed a NLOS UV communication network system, where a beacon-enabled TDMA scheme is adopted. We have also analyzed the existing time delays of the time synchronization and designed algorithms for beacon transmission, time compensation and time slot transition. We have conducted experiments to evaluate the time synchronization error between nodes and the network system is specified based on the experimental results. We have also verified that the network system can work based on the lab test. Furthermore, we have conducted outdoor FOV test to evaluate the FOV of the LEDs and PMTs. Based on the experimental results, we have finished the outdoor field test on the school playground with the transmission range over $110 \times 90 \text{m}^2$, where the system throughput reaches 800kbps.

REFERENCES

- [1] G. A. Shaw, A. M. Siegel, and J. Model, "Extending the range and performance of non-line-of-sight ultraviolet communication links," in *Unattended Ground, Sea, and Air Sensor Technologies and Applications VIII*, vol. 6231. SPIE, 2006, pp. 93–104.
- [2] Z. Xu and B. M. Sadler, "Ultraviolet communications: potential and state-of-the-art," *IEEE Communications Magazine*, vol. 46, no. 5, pp. 67–73, 2008.
- [3] W.-Y. Lin, C.-Y. Chen, H.-H. Lu, C.-H. Chang, Y.-P. Lin, H.-C. Lin, and H.-W. Wu, "10m/500mbps wdm visible light communication systems," *Optics express*, vol. 20, no. 9, pp. 9919–9924, 2012.
- [4] M. A. Khalighi and M. Uysal, "Survey on free space optical communication: A communication theory perspective," *IEEE communications surveys & tutorials*, vol. 16, no. 4, pp. 2231–2258, 2014.
- [5] C.-H. Yeh, L.-Y. Wei, and C.-W. Chow, "Using a single vcsel source employing ofdm downstream signal and remodulated oofdm upstream signal for bi-directional visible light communications," *Scientific reports*, vol. 7, no. 1, p. 15846, 2017.
- [6] W.-C. Wang, C.-W. Chow, L.-Y. Wei, Y. Liu, and C.-H. Yeh, "Long distance non-line-of-sight (nlos) visible light signal detection based on rolling-shutter-patterning of mobile-phone camera," *Optics express*, vol. 25, no. 9, pp. 10 103–10 108, 2017.
- [7] J.-Y. Sung, C.-W. Chow, and C.-H. Yeh, "Is blue optical filter necessary in high speed phosphor-based white light led visible light communications?" *Optics express*, vol. 22, no. 17, pp. 20 646–20 651, 2014.
- [8] A. Vavoulas, H. G. Sandalidis, N. D. Chatzidiamantis, Z. Xu, and G. K. Karagiannidis, "A survey on ultraviolet c-band (uv-c) communications," *IEEE Communications Surveys & Tutorials*, vol. 21, no. 3, pp. 2111–2133, 2019.
- [9] M. R. Frey, "Information capacity of the poisson channel," *IEEE Transactions on Information Theory*, vol. 37, no. 2, pp. 244–256, 1991.
- [10] A. D. Wyner, "Capacity and error exponent for the direct detection photon channel. ii," *IEEE Transactions on Information Theory*, vol. 34, no. 6, pp. 1462–1471, 1988.
- [11] J. Cao, S. Hranilovic, and J. Chen, "Capacity-achieving distributions for the discrete-time poisson channel—part ii: Binary inputs," *IEEE transactions on communications*, vol. 62, no. 1, pp. 203–213, 2013.
- [12] A. Lapidath and S. M. Moser, "On the capacity of the discrete-time poisson channel," *IEEE Transactions on Information Theory*, vol. 55, no. 1, pp. 303–322, 2008.
- [13] S. M. Haas and J. H. Shapiro, "Capacity of wireless optical communications," *IEEE Journal on Selected Areas in communications*, vol. 21, no. 8, pp. 1346–1357, 2003.
- [14] K. Chakraborty, S. Dey, and M. Franceschetti, "Outage capacity of mimo poisson fading channels," *IEEE Transactions on information Theory*, vol. 54, no. 11, pp. 4887–4907, 2008.
- [15] K. Chakraborty and P. Narayan, "The poisson fading channel," *IEEE Transactions on Information Theory*, vol. 53, no. 7, pp. 2349–2364, 2007.
- [16] T. Cao, J. Song, and C. Pan, "Simplified closed-form single-scatter path loss model of non-line-of-sight ultraviolet communications in noncoplanar geometry," *IEEE Journal of Quantum Electronics*, vol. 57, no. 2, pp. 1–9, 2021.
- [17] T. Cao, T. Wu, C. Pan, and J. Song, "Single-collision-induced path loss model of reflection-assisted non-line-of-sight ultraviolet communications," *Optics Express*, vol. 30, no. 9, pp. 15 227–15 237, 2022.
- [18] H. Ding, G. Chen, A. K. Majumdar, B. M. Sadler, and Z. Xu, "Modeling of non-line-of-sight ultraviolet scattering channels for communication," *IEEE journal on selected areas in communications*, vol. 27, no. 9, pp. 1535–1544, 2009.
- [19] H. Qi, D. Zou, C. Gong, and Z. Xu, "Two-dimensional intensity distribution and adaptive power allocation for ultraviolet ad-hoc network," *IEEE Transactions on Green Communications and Networking*, vol. 6, no. 1, pp. 558–570, 2021.
- [20] D. Zou, C. Gong, K. Wang, and Z. Xu, "Characterization on practical photon counting receiver in optical scattering communication," *IEEE Transactions on Communications*, vol. 67, no. 3, pp. 2203–2217, 2018.
- [21] C. Gong and Z. Xu, "Channel estimation and signal detection for optical wireless scattering communication with inter-symbol interference," *IEEE Transactions on Wireless Communications*, vol. 14, no. 10, pp. 5326–5337, 2015.
- [22] D. Zou, C. Gong, and Z. Xu, "Signal detection under short-interval sampling of continuous waveforms for optical wireless scattering communication," *IEEE Transactions on Wireless Communications*, vol. 17, no. 5, pp. 3431–3443, 2018.
- [23] C. Gong, X. Zhang, Z. Xu, and L. Hanzo, "Optical wireless scattering channel estimation for photon-counting and photomultiplier tube receivers," *IEEE Transactions on Communications*, vol. 64, no. 11, pp. 4749–4763, 2016.
- [24] X. Liang, M. Zhang, and D. Han, "Security performance of polar codes in uv wireless communications," in *2018 Asia Communications and Photonics Conference (ACP)*. IEEE, 2018, pp. 1–3.
- [25] C. Gong and Z. Xu, "Temporal spectrum sensing for optical wireless scattering communications," *Journal of Lightwave Technology*, vol. 33, no. 18, pp. 3890–3900, 2015.
- [26] L. Liao, Z. Li, T. Lang, and G. Chen, "Uv led array based nlos uv turbulence channel modeling and experimental verification," *Optics express*, vol. 23, no. 17, pp. 21 825–21 835, 2015.
- [27] K. Wang, C. Gong, D. Zou, and Z. Xu, "Turbulence channel modeling and non-parametric estimation for optical wireless scattering communication," *Journal of Lightwave Technology*, vol. 35, no. 13, pp. 2746–2756, 2017.
- [28] G. A. Shaw, A. M. Siegel, J. Model, A. Geboff, S. Soloviev, A. Vert, and P. Sandvik, "Deep uv photon-counting detectors and applications," in *Advanced Photon Counting Techniques III*, vol. 7320. SPIE, 2009, pp. 88–102.
- [29] G. Chen, L. Liao, Z. Li, R. J. Drost, and B. M. Sadler, "Experimental and simulated evaluation of long distance nlos uv communication," in *2014 9th International Symposium on Communication Systems, Networks & Digital Sign (CSNDSP)*. IEEE, 2014, pp. 904–909.
- [30] A. Lapidath and S. Shamai, "The poisson multiple-access channel," *IEEE Transactions on Information Theory*, vol. 44, no. 2, pp. 488–501, 1998.
- [31] A. Vavoulas, H. G. Sandalidis, and D. Varoutas, "Connectivity issues for ultraviolet uv-c networks," *Journal of Optical Communications and Networking*, vol. 3, no. 3, pp. 199–205, 2011.
- [32] M. H. Ardakani and M. Uysal, "Relay-assisted ofdm for ultraviolet communications: performance analysis and optimization," *IEEE Transactions on Wireless Communications*, vol. 16, no. 1, pp. 607–618, 2016.
- [33] M. H. Ardakani, A. R. Heidarpour, and M. Uysal, "Performance analysis of relay-assisted nlos ultraviolet communications over turbulence channels," *Journal of Optical Communications and Networking*, vol. 9, no. 1, pp. 109–118, 2017.
- [34] G. Wang, C. Gong, and Z. Xu, "Signal characterization for multiple access non-line-of-sight scattering communication," *IEEE Transactions on Communications*, vol. 66, no. 9, pp. 4138–4154, 2018.
- [35] C. Gong, Q. Gao, and Z. Xu, "Signal detection for superposition transmission protocols for optical wireless scattering broadcast channel," *IEEE Transactions on Wireless Communications*, vol. 17, no. 8, pp. 5480–5493, 2018.
- [36] G. Wang, K. Wang, C. Gong, D. Zou, Z. Jiang, and Z. Xu, "A 1mbps real-time nlos uv scattering communication system with receiver diversity over 1km," *IEEE Photonics Journal*, vol. 10, no. 2, pp. 1–13, 2018.